Blind Deblurring for Saturated Images

Liang Chen [*1], Jiawei Zhang [†2], Songnan Lin[2], Faming Fang[1], Jimmy S. Ren[2,3]
[1] Shanghai Key Laboratory of Multidimensional Information Processing,
School of Computer Science and Technology, East China Normal University
[2] SenseTime Research
[3] Qing Yuan Research Institute, Shanghai Jiao Tong University, Shanghai, China

Abstract

Blind deblurring has received considerable attention in recent years. However, state-of-the-art methods often fail to process saturated blurry images. The main reason is that pixels around saturated regions are not conforming to the commonly used linear blur model. Pioneer arts suggest excluding these pixels during the deblurring process, which sometimes simultaneously removes the informative edges around saturated regions and results in insufficient information for kernel estimation when large saturated regions exist. To address this problem, we introduce a new blur model to fit both saturated and unsaturated pixels, and all informative pixels can be considered during the deblurring process. Based on our model, we develop an effective maximum a posterior (MAP)-based optimization framework. Quantitative and qualitative evaluations on benchmark datasets and challenging real-world examples show that the proposed method performs favorably against existing methods.

1. Introduction

At night, a long exposure is often required to capture the dark regions and it often results in heavy blur in the captured image due to the inevitable camera shake. Meanwhile, because of the existence of lights at night, the images also commonly contain saturated regions. As a result, the images captured at night are usually blurry and partially saturated at the same time.

Mathematically, the widely adopted linear blurring process can be modeled by convolving a sharp image I with a blur kernel K:

$$B = I \otimes K, \tag{1}$$

where B is the blurry image and $\otimes$ denotes the convolution operation. Recovering the latent sharp image given only a single blurry image, which is referred to as blind deblurring, has long been a fundamental research problem in the image processing community.

Based on the degrading model in Eq. (1), significant efforts [9, 29, 14, 34, 25, 10, 35, 23, 18, 3, 2] have been proposed in recent years. Despite their effectiveness in most occasions, these methods often have difficulties recovering a blurry image with saturated regions as shown in Figure 1 (b) and (c). The major reason lies in that the saturated pixels tend to violate the linear blur model in Eq. (1), and it will mislead the kernel estimation process during deblurring [6, 7, 4].

Considering this, existing algorithms [24, 7, 4] suggest implicitly or explicitly excluding the saturated pixels during the deblurring process. Specifically, Pan *et al*. [24] select salient edges from unsaturated areas and use them to improve the kernel estimation, while Dong *et al*. [7] and Chen *et al*. [4] both suggest using sophisticated fidelity term so that only unsaturated pixels can contribute during deblurring. However, these methods are only effective in blurry images with small saturated regions. When the saturated regions are large (Figure 1 (a)), all of them will encounter setbacks as shown in Figure 1 (d), (e) and (f). As there are not enough informative pixels left to estimate the kernel when the sharp, strong edges of the light streaks are discarded in their methods.

To acquire enough information to estimate the blur kernel while avoiding the side-effects brought by the saturated pixels, we propose a simple yet effective blur model that considers both saturated and unsaturated pixels. Specifically, we introduce a latent map M into the blur model in Eq. (1). For a pixel i, the latent map assures that the degrading process (*i.e.* $M_i(I \otimes K)_i$) can output values within the sensor range[1]. Our proposed latent map serves similarly as an ideal clipping function in [6, 32] (*i.e.* $\min((I \otimes K)_i, 1)$). Different from the clipping function, our latent map-based model is differentiable, which enables the further optimization process. Based on the proposed blur model, we develop

---

*This work was done when Liang Chen was an intern at SenseTime.
†Corresponding author

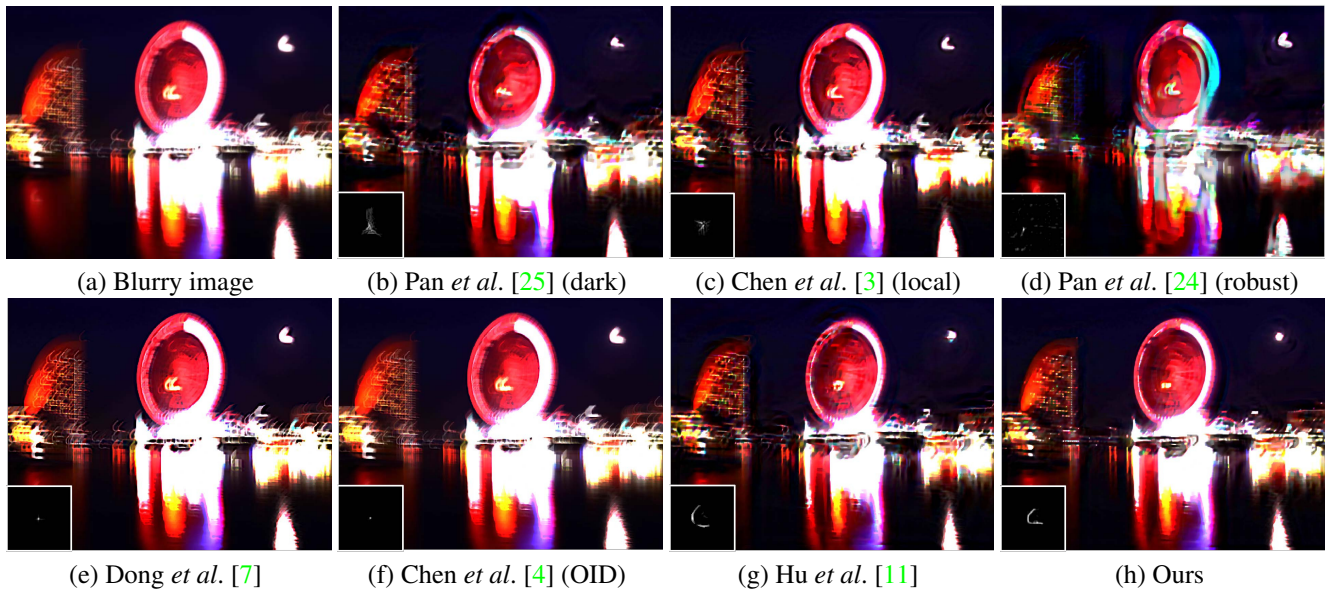[1]The maximum value of the sensor range is 1 in our setting.

Figure 1. Deblurring results of a saturated blurry image. Estimated kernels are shown in the white boxes. Methods based on Eq. (1) [25, 3] fail to accurately estimate the kernel. The robust models [24, 7, 4] exclude saturated pixels during the deblurring process, and they are also ineffective when there present large saturated regions. When the light streaks are difficult to extract, [11] also does not work well. In comparison, the proposed method can generate a high-quality result with fewer artifacts.

an efficient MAP-based optimization framework to estimate both the latent image as well as the blur kernel. Qualitative and quantitative experiments on extensive examples show the superiority of the proposed model against the state-of-the-art algorithms.

The main contributions of this work are as follows:

- We propose a new blur model by introducing a latent map into the commonly used linear blur model. Without any heuristic settings, the proposed model can take advantage of both saturated and unsaturated pixels during the deblurring process.

- We develop an effective MAP-based deblurring framework based on the proposed degrading model. Further analyses show that our framework converges well in a few iterations and requires less processing time than existing methods.

- The experimental results on the benchmark datasets [11, 13, 23] and real-world images demonstrate that our method performs favorably against state-of-the-art methods both quantitatively and qualitatively.

2. Related Works

Blind deblurring is a highly ill-posed problem. There have been numerous advances made in recent years to solve this problem [29, 34, 25, 35, 23, 31, 15, 37, 3, 2, 19]. However, these methods will generate severe ringing artifacts when there are saturated regions in the blurry image.

Deblurring with saturated pixels is a challenging issue in real life, and most blind deblurring methods [24, 7, 4] are

based on the pioneer arts that are developed for non-blind deblurring [6, 32]. Cho et al. [6] suggest regarding pixels around saturated regions and impulsive noises as outliers. They propose an expectation-maximization method to iteratively detect the outliers and use the inliers to estimate the latent image. Whyte et al. [32] use a differentiable function to approximate the clipping function. During their optimization process, the saturated pixels hardly influence the deblurred images.

Based on the above idea that excluding the outliers, some blind deblurring algorithms are developed. Pan et al. [24] first use an edge selecting strategy to find informative edges during the latent image estimation step, and then they use the detected inliers to refine the blur kernel. Instead of detecting outliers directly, Dong et al. [7] use a sophisticated data fidelity term to suppress the side effect brought by outliers during deblurring steps. In addition, Chen et al. [4] suggest explicitly identifying outliers more faithfully and discarding them during both the kernel and latent image refining steps. However, the pixels around saturated regions can sometimes provide useful information, such as sharp edges, for the kernel estimation, and simply discarding outliers in these methods will result in insufficient details to estimate the correct kernel when there are large saturated regions. Moreover, the above mentioned methods require heuristic settings to identify saturated pixels. Another perspective comes from [11]. Hu et al. suggest using light streaks that appeared in the low-light images. Their method is effective in most cases. However, the light streaks are only useful when the light sources are point lights and it fails when the light sources are large (Figure 1 (g)).

With the development of the convolution neural network (CNN), numerous deep learning-based deblurring methods are recently developed [21, 22, 31, 38, 15, 37, 26]. These approaches take advantage of the large learning capacity of the neural networks and show their effectiveness in most cases. However, the learning-based methods neglect the contribution from a proper imaging process and they are likely to perform less effective for severe blur.

3. Our Method

3.1. Proposed blur model

Images taken under the low-light condition often do not contain enough informative details to estimate the blur kernels [11], and simply using the edges from the saturated regions without proper procedure will cause problems for both blur kernel and deblurred image estimation [6]. Thus, to ensure that the deblurring process can benefit from both saturated and unsaturated information, our goal is to develop a blur model that fits all pixels as:

$$B = M \circ (I \otimes K)$$
$$\text{s.t. } M_i = \begin{cases} 1, & \text{if } (I \otimes K)_i \leq 1 \\ \frac{1}{(I \otimes K)_i}, & \text{Otherwise} \end{cases} \quad (2)$$

in which M is a latent map and $\circ$ denotes the Hadamard multiplication. In this way, M serves similarly as a clipping function [6, 32] and keeps the blurry image within the maximum value of the sensor range. Also, compared to [32] that approximates the clipping function, the proposed latent map is easy to implement and does not require any heuristic settings in our blur model.

3.2. Optimization procedures

Based on the proposed blur model in Eq. (2), we use a MAP-based scheme to estimate the latent image and blur kernel as:

$$\min_{I,K} \mathcal{L}(B, M \circ (I \otimes K)) + \lambda P_I(I) + \beta P_K(K), \quad (3)$$

where $\mathcal{L}$ is the fidelity term that enforces the similarity between the blurry image and the convolution output of the recovered image and the blur kernel; P_I and P_K are prior terms imposed on the latent image and blur kernel; λ and β are the weights.

The same with [32, 36, 30], we assume the imaging process follows the Poisson distribution and the fidelity term can be presented as:

$$\mathcal{L}(B, M \circ (I \otimes K))$$
$$= -\log \prod_i \mathcal{P}oisson(B_i; M_i(I \otimes K)_i) \quad (4)$$
$$= M \circ (I \otimes K) - \log(M \circ (I \otimes K)) \circ B,$$

where $\mathcal{P}oisson(\bullet; \sigma^2)$ is the Poisson distribution with parameter σ^2. Note the constant is discarded since it does not influence the minimization.

Similar to [7, 4], we use the hyper-Laplacian prior [16] for P_I (i.e. $P_I(I) = \|\nabla I\|_{0.8}$, where ∇ is the gradient operator in horizontal and vertical dimensions, and smooth prior for P_K (i.e. $P_K(K) = \|K\|^2$).

We solve Eq. (3) by alternatively updating I and K with the other one fixed. The sub-problems referring to I and K is given by,

$$\begin{cases} \min_I \mathcal{L}(B, M \circ (I \otimes K)) + \lambda P_I(I), & (5) \\ \min_K \mathcal{L}(B, M \circ (I \otimes K)) + \beta P_K(K), & (6) \end{cases}$$

Solving the problem referring to I. We can minimize Eq. (5) by setting its derivative to zero as:

$$M \otimes \widetilde{K} - \frac{M \circ B}{M \circ (I \otimes K)} \otimes \widetilde{K} + \lambda P_I'(I) = 0, \quad (7)$$

where $\widetilde{K}$ is the transpose of K that flips the shape of K upside down and left-to-right, $P_I'(I)$ is the first order derivative of $P_I(I)$ w.r.t. I, and $P_I'(I) = sgn(\nabla_h I)0.8|\nabla_h I|^{-0.2} + sgn(\nabla_v I)0.8|\nabla_v I|^{-0.2}$, where $sgn(\bullet)$ is the sign function. The division operation here is element-wise.

Based on Eq. (7), we can obtain I using the Richardson-Lucy updating scheme [27, 20], which further gives,

$$I^{t+1} = \frac{I^t \circ ((\frac{B}{I^t \otimes K} - M + \mathbf{1}) \otimes \widetilde{K})}{\mathbf{1} + \lambda P_I'(I^t)}, \quad (8)$$

where t denotes the updating index, $\mathbf{1}$ is the all-one matrix. Note that in each updating step, the latent map M should be computed as defined in Eq. (2) after every updating step of I^t (i.e. $M_i = 1$, if $(I^t \otimes K)_i \leq 1$; or $M_i = 1/(I^t \otimes K)_i$, if $(I^t \otimes K)_i > 1$).

Details can be found in our supplementary material.
Solving the problem referring to K. However, it is inappropriate to update the blur kernel K with the Richardson-Lucy scheme[2]. To make the problem tractable, we use the approximation rule in [8] that for $\forall \sigma$, we have,

$$\mathcal{P}oisson(\bullet; \sigma^2) \approx \mathcal{N}(\bullet; \sigma^2, \sigma^2), \quad (9)$$

where $\mathcal{N}(\bullet; \sigma^2, \sigma^2)$ is the Gaussian distribution with both mean and variance equal to σ^2. Then the fidelity term in Eq. (6) can be represented as:

$$\mathcal{L}(B, M \circ (I \otimes K))$$
$$= -\log \prod_i \mathcal{N}(B_i; M_i(I \otimes K)_i, M_i(I \otimes K)_i)$$
$$= -\log \prod_i \mathcal{N}(B_i - M_i(I \otimes K)_i; 0, W_{i,i}^{-1}) \quad (10)$$
$$\text{s.t. } W^{-1} = diag(M \circ (I \otimes K))$$

---
[2]Please see supplemental material for analysis.

According to [1], based on the Gauss-Markov theorem, we can rewrite the above formation into,

$$\mathcal{L}(B, M \circ (I \otimes K)) = \|B - M \circ (I \otimes K)\|_W^2 + C, \quad (11)$$

where $\| \bullet \|_W^2$ is the norm under metric W, and C is a constant.

As demonstrated in [5, 34, 25], the estimation based on image gradients is more stable and accurate. Based on Eq. (6), we can estimate the blur kernel K by minimizing:

$$\min_K \|\nabla B - M \circ (\nabla I \otimes K)\|_W^2 + \beta \|K\|^2. \quad (12)$$

The above formation is a weighted least square problem. Following the optimization in [4] which uses an iteratively updating strategy to solve the weighted least square problem, we estimate the blur kernel K by alternately minimizing Eq. (12) using conjugate gradient method and computing the weighted matrix W using Eq. (11). The latent map M is also computed after updating the kernel as defined in Eq. (2). As the blur kernel should be non-negative and sum to 1, we set the negative elements of K to 0, and normalize it to make its summation equal to 1 after estimating K.

Details can be found in our supplemental material.

3.3. Overall algorithm

The overall deblurring process is implemented in a coarse-to-fine manner using an image pyramid [5]. We construct the image pyramid B_1, B_2, ..., B_L from the blurred image B where $B_1 = B$ and B_L is the coarsest down-sampled version of B. The computation for the kernel and the intermediate latent image starts from the coarsest level L, and the obtained kernel K_L is then up-sampled and used as the initialization for the next level (*i.e.* level $L - 1$). The main steps of our blind deblurring method in one pyramid level are shown in Algorithm 1. After the kernel is obtained from the finest scale (*i.e.* level 1), we apply the non-blind deblurring method derived from Eq. (5) to recover the final deblurred image.

4. Experiments

In this section, we evaluate the performance of the proposed method on both synthetic and real images and compare it with different state-of-the-art methods. We first examine our method through extensive numerical experiments on two benchmark datasets with saturated pixels [11, 23] and compare it to the state-of-the-art algorithms. Then, we use some challenging real-world examples with large saturated regions to show the effectiveness of our algorithm. Finally, we use the natural benchmark dataset [13] without saturated pixels to further evaluate the proposed method. All the color images are converted to grayscale ones in the kernel estimation process. In the final image deblurring process, each color channel is processed independently. Due to

---

Algorithm 1 Blind deblurring for saturated images
Input: blurred image B, parameters λ, β and initial kernel $K^{0,0}$.
Output: blur kernel K and intermediate latent image I.
1: Initialize $M^0 = \mathbf{1}$, $I^{0,0} = B$.
2: t=1, x=1, j=0.
3: **while** $j < j_{max}$ **do**
4:     **while** $t < t_{max}$ **do**
5:         Compute $I^{t,j}$ using Eq. (8) given M^{t-1} and K;
6:         Update M^t using Eq. (2) given $I^{t,j}$ and K;
7:         $t \leftarrow t + 1$
8:     **end while**
9:     **while** Stopping criterion is not satisfied **do**
10:         Update W^x using Eq. (11) given $K^{x-1,j}$ and M^x;
11:         Compute $K^{x,j}$ using Eq. (12) given W^x and M^x;
12:         Update M^x using Eq. (2) given $K^{x-1,j}$ and I;
13:         $x \leftarrow x + 1$;
14:     **end while**
15:     $j \leftarrow j + 1$
16: **end while**

---

the comprehensive experiments performed, we only demonstrate a small portion of the results in the main manuscript. Please refer to the supplementary material for more experimental results.

Our method is implemented in the MATLAB platform on a computer with an Intel Core i5 CPU and 8 GB RAM. In all experiments, we fix the parameters as $\lambda = 0.008$, $\beta = 2$. We set the maximum outer iteration $j_{max} = 4$ and set the maximum inner iteration for updating the latent image $t_{max} = 50$ in each level of Algorithm 1. For the sub-problem referring to update K, we set the stopping criterion to be that if the relative error between successive iterates is smaller than 10^{-3}.

4.1. Saturated dataset from Hu *et al.* [11]

The saturated dataset provided by Hu *et al.* [11] contains 11 images and 14 blur kernels. We compare our method with the competing methods including the optimization-based ones [11, 24, 7, 4] that are designed for saturated blurry images, and the learning-based algorithms [31, 15] which are fine-tuned using the real-world data from [28][3]. When the kernels are estimated by different optimization-based methods, we use the same non-blind deblurring method derived from Eq. (5) to obtain the final results. PSNR and SSIM are used to evaluate the performance. As shown in Figure 2 and Table 1, our method achieves the highest average PSNR and SSIM values among all the methods evaluated. A challenging example from this

---

[3]The compared learning-based models are the top two best algorithms after fine-tuning with the provided data according to http://cg.postech.ac.kr/research/realblur/.
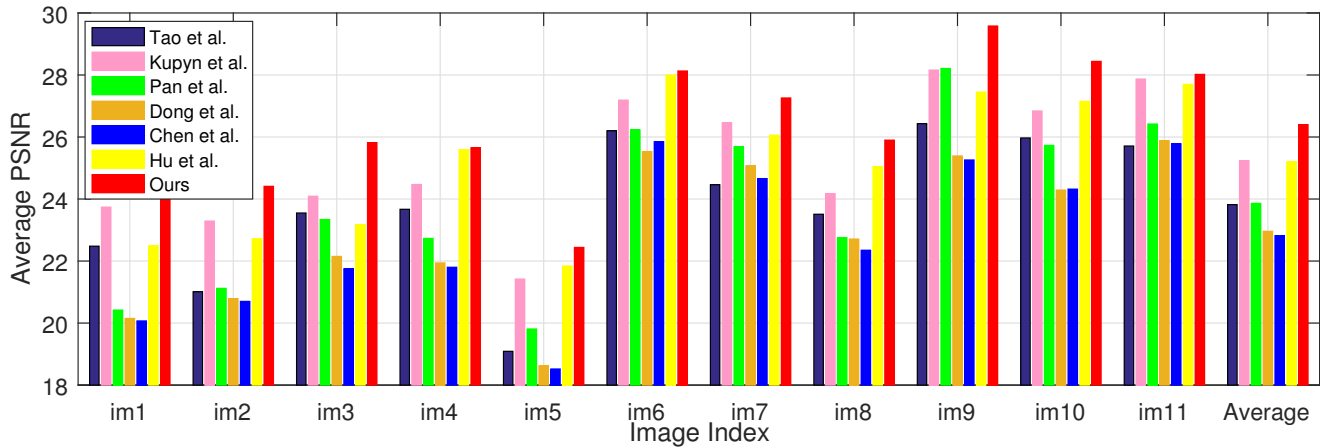
Figure 2. Average PSNR values on the saturated dataset [11]. Our method performs the best among the compared methods.

	Tao *et al*. [31]	Kupyn *et al*. [15]	Pan *et al*. [24]	Dong *et al*. [7]	Chen *et al*. [4]	Hu *et al*. [11]	Ours
Average SSIM	0.7812	0.7980	0.7605	0.7485	0.7509	0.7856	0.8098

Table 1. Average SSIM values on the saturated dataset [11]. Our method performs the best among the compared methods.

(a) Blurred image   (b) Tao *et al*. [31]   (c) Kupyn *et al*. [15]   (d) Pan *et al*. [24]

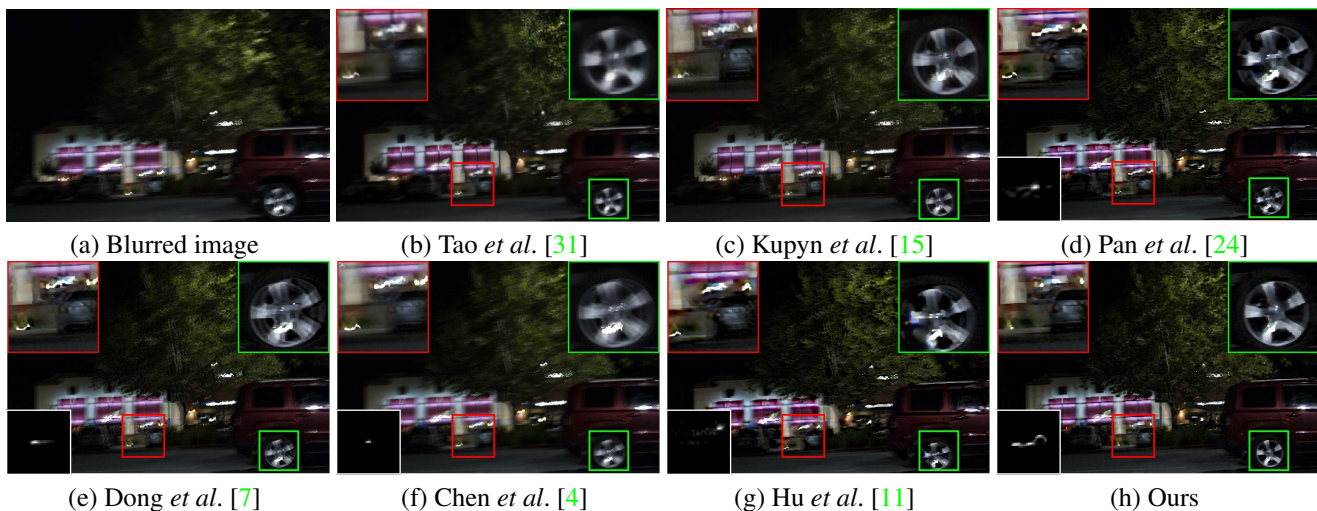(e) Dong *et al*. [7]   (f) Chen *et al*. [4]   (g) Hu *et al*. [11]   (h) Ours

Figure 3. A challenging example from the saturated dataset [11]. Our method generates a result with sharper edges and fewer artifacts as depicted in the boxes. (Best viewed on a high-resolution display with zoom-in.)

dataset is shown in Figure 3, where most state-of-the-art methods [11, 4, 24, 7] fail to estimate decent blur kernels due to large saturated regions, and the learning-based methods [31, 15] also generate results with large blur. In contrast, the results from our method are with finer details.

4.2. Low-light dataset from Pan *et al*. [23]

To further evaluate the effectiveness of our method, we test it on the low-light dataset constructed by Pan *et al*. [23], which contains 6 ground truth images and 8 blur kernels from [17]. We compare our method with the aforementioned robust optimization-based methods [24, 7, 4] and the learning-based approaches [31, 15]. Note that most images from this dataset do not contain detectable light streaks.

Thus, we do not compare with the method from [11] in this dataset since it fails in most cases. The same non-blind method from Eq. (5) is used to restore the final image for the optimization-based models. We use the error ratio [17] as the quality metric. As illustrated in Figure 4 (a), our method achieves the best performance among the methods evaluated with 100% of the error ratio under 2, while the second best [31] is 68.8%.

4.3. Real-world examples

Here we use some real-world images to evaluate the proposed method against the state-of-the-art methods [11, 25, 24, 7, 3, 4, 31, 15]. Figure 5 and 6 show two challenging real examples with abundant saturated pixels. As depicted
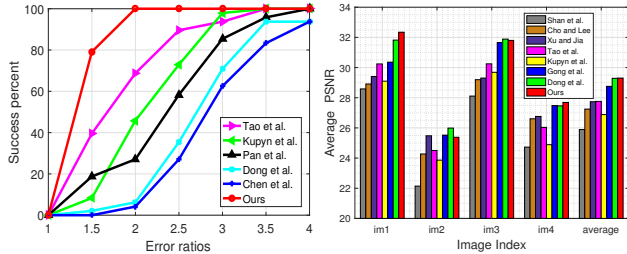
(a) Results on dataset [23]   (b) Results on dataset [13]

Figure 4. Quantitative evaluations of the proposed method on benchmark datasets [23, 13]. Our method performs competitively against state-of-the-art methods.

(a) Input   (b) Pan *et al*. [24]   (c) Chen *et al*. [3]

(d) Kupyn *et al*. [15] (e) Hu *et al*. [11]   (f) Our result

Figure 5. Qualitative evaluations on a challenging real-world example. The parts in red and green boxes in (b)-(e) still contain ringings and large blur.

in the figures, state-of-the-art methods [25, 3] are ineffective due to the side-effects brought by the saturated pixels. The robust methods [24, 7, 4] do not perform well when the blurry images contain large saturated regions. Their deblurred results contain ringing artifacts, and some details are not recovered well (Figure 5 (b) and Figure 6 (d) - (f)). Hu *et al*. [11] is unable to estimate the correct blur kernels when salient light streaks are unavailable in the blurred images. As a result, their results contain unnatural colors in the boxes. In addition, the learning-based approach [15] also encounters setbacks in the given example, and the blur is not fully removed in their result. The most probable reason is that the generalization of the neural network is somehow limited and the blur model is not considered in their network. In contrast, our method successfully estimates the blur kernels and generates high-quality deblurred images.

4.4. Dataset [13] without saturated pixels

As can be inferred by our blur model in Eq. (2), it is also capable of deblurring images without saturated pixels. We conduct experiments on the benchmark dataset provided by Köhler *et al*. [13] which contains 4 clear images and 12 blur kernels. We compare our method with the state-of-the-art

(a) Input   (b) [25]   (c) [3]   (d) [24]

(e) [7]   (f) [4]   (g) [11]   (h) Ours

Figure 6. A real-world example with large saturated regions. The parts in red boxes in (b)-(g) contain ringings and large blur.

general image deblurring methods [29, 5, 33, 10, 7, 31, 15]. After the blur kernels are estimated by different methods, we use the same non-blind deblurring method from [23] to restore the final deblurred images. We use PSNR to evaluate performance, and the PSNR value of each restored image is computed by selecting the highest value relative to 199 clean images captured along the camera motion trajectory. As shown in the histogram in Figure 4 (b), our method performs favorably among all the methods evaluated, which demonstrates the effectiveness of the proposed method on images without saturating.

5. Analysis

5.1. Effectiveness of the proposed latent map

Without considering the latent map, *e.g*. setting $M = 1$, the proposed blur model in Eq. (2) reduces to the formation in Eq. (1). This blur model is widely adopted in many existing methods [34, 25, 3]. However, the deblurred image without the latent map contains severe ringing artifacts in Figure 7 (b). For the proposed latent map M, it is only effective in the proposed blur model when the pixel value of the latent map is less than 1. As shown in Figure 7 (l), the region $M < 1$ is consistent with the saturated region while $M = 1$ is with unsaturated pixels. With the help of this latent map, the intermediate image in Figure 7 (h) contains fewer ringings around the saturated region compared to that without it (Figure 7 (g)), which facilitates the following kernel estimation. As a result, the model with the latent map can generate a result with less blur and fewer ringing artifacts as shown in Figure 7 (f).

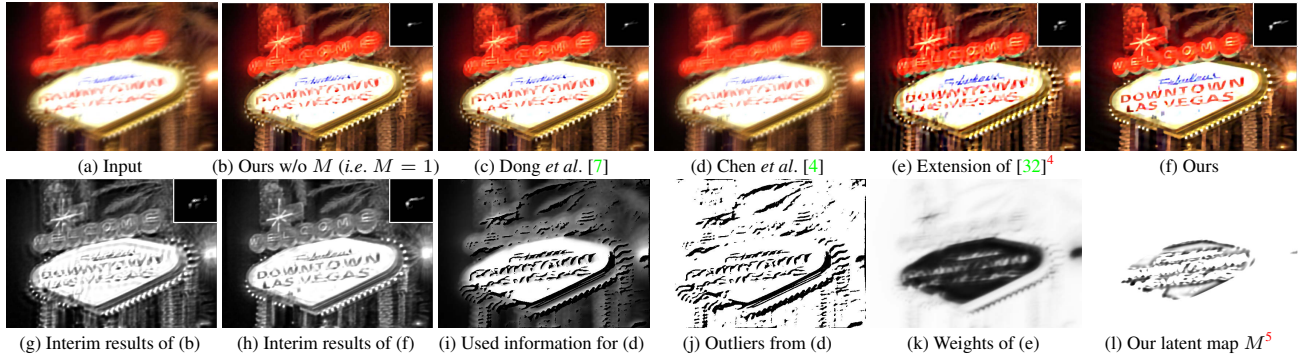To quantitatively compare our method with the strategy

| (a) Input | (b) Ours w/o M (*i.e.* $M = 1$) | (c) Dong *et al.* [7] | (d) Chen *et al.* [4] | (e) Extension of [32][4] | (f) Ours |

| (g) Interim results of (b) | (h) Interim results of (f) | (i) Used information for (d) | (j) Outliers from (d) | (k) Weights of (e) | (l) Our latent map M[5] |

Figure 7. Comparisons between different blur models. During the optimization process, the intermediate latent image I (*i.e.* (g)) without considering the latent map M contains more artifacts than that with it (*i.e.* (h)). The saturated regions from [7, 4] (*i.e.* W in [4]) are detected based on the residual between the blurred image and the convolving result (*i.e.* $B - I \otimes K$), and salient edges from saturated regions are more likely to be detected (darker regions in (j)). Both [7, 4] discard the detected regions in their optimization, and (i) is the remaining image structures (*i.e.* $W \circ B$) used for deblurring in [4] after discarding the outliers. The extension of [32] also excludes saturated pixels including salient edges in their model by implicitly assigning small weights (*e.g.* (k)), which is based on the derivation of approximation function, to these pixels. By considering all the pixels, the proposed method has more information to estimate the blur kernel and generate a shaper result without artifacts (*e.g.* (f)). Please see Sec. 5 for more details.
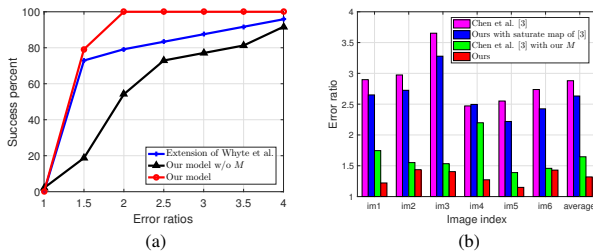

Figure 8. Quantitative evaluations on the dataset [23]. (a) Results w/ (ours), w/o the latent map and using approximation function to replace the latent map (Extension of [32]). (b) Results for different methods (ours and [4]) with different map settings.

that without the latent map, we conduct an ablation study with the low-light dataset in [23]. The results in Figure 8 (a) (red and black lines) show that the proposed latent map consistently improves deblurring, where the success rate of using the latent map is higher than that without it.

5.2. Relation with existing methods

Relation with Dong *et al*. [7] and Chen *et al*. [4] Both of them suggest regarding saturated pixels as outliers which are discarded during their deblurring processes. Our method differs from these methods in the following aspects.

First, these two methods suggest that the saturated pixels are not conforming to their degrading model. In comparison, both saturated and unsaturated pixels conform to our degrading model in Eq. (2). Second, they use an extra step to locate and discard the pixels around saturated regions in the blurred image, explicitly or implicitly. Specifically, their detecting steps rely on the estimation residual $B - I \otimes K$.

---

[4][32] is developed for non-blind deblurring, and we replace our latent map with their clipping approximation function in our blur model for blind deblurring.

[5]The latent map is processed with a gamma correction for a better view.

Pixels with larger residual values are more likely to be saturated [4]. Then, a weight map (*i.e.* W in [4]), which has small values corresponding to the detected region, is used in the deblurring model to assure that outliers do not contribute to the optimization process (*i.e.* $W \circ (B - I \otimes K)$). However, the detected region is more likely to be sharp edges around the saturated regions as shown in Figure 7 (j). As these informative edges in the blurry image are discarded, there may not be enough information left for the deblurring process (Figure 7 (i)). Differently, all the pixels can be considered during our optimization process, which alleviates the limitation in [4, 7] when the remaining information is insufficient to estimate a more accurate kernel.

To compare the weight map in [4] and the proposed latent map, we conduct an ablation study on [23] with different settings in term of error ratio [17]. As shown in Figure 8 (b), the proposed latent map can consistently improve deblurring. The example given in Figure 7 also illustrates the difference between these models. As shown in Figure 7 (c) and (d), their methods fail to obtain a decent blur kernel when using only limited image structures (Figure 7 (i)). Differently, our method takes advantage of both saturated and unsaturated pixels during the deblurring process, and as a result, the deblurred result from our method is with fewer artifacts (Figure 7 (f)). Please refer to our supplementary material for details.

Relation with Whyte *et al*. [32]. [32] is used for non-blind deblurring. Different from our method, they use a sophisticated function to approximate the ideal clipping function. Their approximation requires heuristic parameter settings to control the smoothness of the approximation which may be inappropriate for different images. Further, the derivation of the approximation often has small values corresponding to the saturated regions and it can be approximately consid-
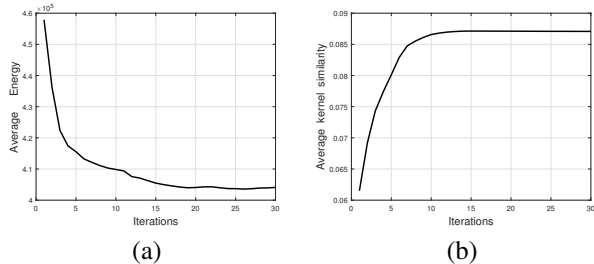
Figure 9. Convergence property of the proposed optimization framework. (a) Energy value of the objective function in Eq. (5). (b) Average kernel similarity [12].

Method	255×255	600×600	800×800
Hu *et al*. [11]	27.28	86.05	198.60
Pan *et al*. [24]	180.10	625.74	1147.50
Dong *et al*. [7]	88.08	667.51	1249.49
Chen *et al*. [4]	52.65	320.62	544.29
Ours	12.03	76.05	143.26

Table 2. Running time comparison on images with different sizes. The codes are all implemented in MATLAB.

ered as assigning small weights to the saturated pixels similar to [7, 4] during their deblurring process. Consequently, they also only use unsaturated pixels for the deblurring.

For comparison, we extend [32] to blind deblurring by replacing our latent map with their approximation function in both the latent image and blur kernel estimation processes of our deblurring framework. The example presented in Figure 7 (e) shows the restored result contains blur and artifacts. The main reason is that most saturated pixels, including the salient edges, are discarded in their model (Figure 7 (k)). Consequently, there will be insufficient information to estimate the blur kernel when large regions in the blurry image are saturated. The quantitatively results in Figure 8 (a) (blue line) also show that their approximation is less effective than our method, where the success rate of using the proposed latent map is higher than replacing it with the approximation function. This validates the superiority of our method over the extension of [32].

5.3. Convergence property

We evaluate the convergence property of our optimization framework using the low-light dataset [23]. We compute the output of the energy function in Eq. (5) and the kernel similarity [12] referring to Eq. (6), and they are both measured at the finest image scale. Results shown in Figure 9 (a) and (b) demonstrate that our optimization framework converges less than 30 iterations, which validates the effectiveness of our optimization scheme.

5.4. Running time comparison

In addition, we also compare the average running time between some optimization based methods. Experiments are conducted on images of different sizes. The overall
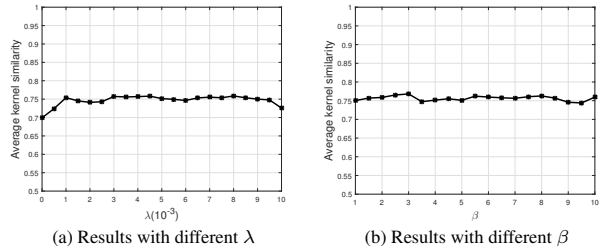

Figure 10. Sensitivity analysis of the parameters λ and β on the proposed algorithm.

results are shown in Table 2. Our method achieves the fastest running time among the algorithms evaluated because it does not involve any preprocess steps or edge selecting strategies.

5.5. Parameter analysis

The proposed model involves two parameters λ and β. We evaluate the effects of these parameters on image deblurring in the dataset from [23].

Figure 10 (a) shows that the kernel can be well estimated by a wide range of λ (*i.e.* from 0.001 to 0.01), and the results in Figure 10 (b) demonstrate that the proposed framework can output decent results with a wide range of parameter settings of β. The analysis demonstrates that our model performs well in a wide range of hyper-parameter settings.

6. Conclusion

In this paper, we develop a new method to restore saturated blurred images. We first propose a new blur model that takes both saturated and unsaturated pixels into account. Unlike previous approaches, the strong edges around the saturated regions can still contribute to the deblurring process, which alleviates the limitation of existing methods when large saturated regions are present in the blurred image. Then, based on the proposed blur model, we develop an efficient MAP-based optimization framework, which is shown to converge well and requires less execution time than other methods. Experimental results demonstrate that the proposed method performs favorably against state-of-the-art methods without additional pre-processing steps (*i.e.* extracting light streaks or selecting salient edges), and it can obtain high-quality results on challenging real examples.

Acknowledgements

References

[1] Johnathan M Bardsley and James G Nagy. Covariance-preconditioned iterative methods for nonnegatively constrained astronomical imaging. *SIAM journal on matrix analysis and applications*, 27(4):1184–1197, 2006. 4

[2] Liang Chen, Fang Faming, Shen Lei, Fang Li, and Guixu Zhang. Enhanced sparse model for blind deblurring. In *ECCV*, 2020. 1, 2

[3] Liang Chen, Faming Fang, Tingting Wang, and Guixu Zhang. Blind image deblurring with local maximum gradient prior. In *CVPR*, 2019. 1, 2, 5, 6

[4] Liang Chen, Faming Fang, Jiawei Zhang, Jun Liu, and Guixu Zhang. Oid: Outlier identifying and discarding in blind image deblurring. In *ECCV*, 2020. 1, 2, 3, 4, 5, 6, 7, 8

[5] Sunghyun Cho and Seungyong Lee. Fast motion deblurring. *ACM ToG*, 28(5):145, 2009. 4, 6

[6] Sunghyun Cho, Jue Wang, and Seungyong Lee. Handling outliers in non-blind image deconvolution. In *ICCV*, 2011. 1, 2, 3

[7] Jiangxin Dong, Jinshan Pan, Zhixun Su, and Ming-Hsuan Yang. Blind image deblurring with outlier handling. In *ICCV*, 2017. 1, 2, 3, 4, 5, 6, 7, 8

[8] William Feller. An introduction to probability theory and its applications. *1957*. 3

[9] Robert Fergus, Barun Singh, Aaron Hertzmann, Sam T. Roweis, and William T. Freeman. Removing camera shake from a single photograph. *ACM ToG*, 25(3):787–794, 2006. 1

[10] Dong Gong, Mingkui Tan, Yanning Zhang, Anton van den Hengel, and Qinfeng Shi. Blind image deconvolution by automatic gradient activation. In *CVPR*, 2016. 1, 6

[11] Zhe Hu, Sunghyun Cho, Jue Wang, and Ming-Hsuan Yang. Deblurring low-light images with light streaks. In *CVPR*, 2014. 2, 3, 4, 5, 6, 8

[12] Zhe Hu and Ming-Hsuan Yang. Good regions to deblur. In *ECCV*, 2012. 8

[13] Rolf Köhler, Michael Hirsch, Betty Mohler, Bernhard Schölkopf, and Stefan Harmeling. Recording and playback of camera shake: Benchmarking blind deconvolution with a real-world database. In *ECCV*, 2012. 2, 4, 6

[14] Dilip Krishnan, Terence Tay, and Rob Fergus. Blind deconvolution using a normalized sparsity measure. In *CVPR*, 2011. 1

[15] Orest Kupyn, Tetiana Martyniuk, Junru Wu, and Zhangyang Wang. Deblurgan-v2: Deblurring (orders-of-magnitude) faster and better. In *ICCV*, 2019. 2, 3, 4, 5, 6

[16] Anat Levin, Robert Fergus, Frédo Durand, and William T. Freeman. Image and depth from a conventional camera with a coded aperture. *ACM ToG*, 26(3):70, 2007. 3

[17] Anat Levin, Yair Weiss, Fredo Durand, and William T Freeman. Understanding and evaluating blind deconvolution algorithms. In *CVPR*, 2009. 5, 7

[18] Lerenhan Li, Jinshan Pan, Wei-Sheng Lai, Changxin Gao, Nong Sang, and Ming-Hsuan Yang. Learning a discriminative prior for blind image deblurring. In *CVPR*, 2018. 1

[19] Jun Liu, Ming Yan, and Tieyong Zeng. Surface-aware blind image deblurring. *IEEE TPAMI*, 43(3):1041–1055, 2021. 2

[20] Leon B Lucy. An iterative technique for the rectification of observed distributions. *The astronomical journal*, 79:745, 1974. 3

[21] Seungjun Nah, Tae Hyun Kim, and Kyoung Mu Lee. Deep multi-scale convolutional neural network for dynamic scene deblurring. In *CVPR*, 2017. 3

[22] Thekke Madam Nimisha, Akash Kumar Singh, and Ambasamudram N Rajagopalan. Blur-invariant deep learning for blind-deblurring. In *CVPR*, 2017. 3

[23] Jinshan Pan, Zhe Hu, Zhixun Su, and Ming-Hsuan Yang. l_0-regularized intensity and gradient prior for deblurring text images and beyond. *IEEE TPAMI*, 39(2):342–355, 2017. 1, 2, 4, 5, 6, 7, 8

[24] Jinshan Pan, Zhouchen Lin, Zhixun Su, and Ming-Hsuan Yang. Robust kernel estimation with outliers handling for image deblurring. In *CVPR*, 2016. 1, 2, 4, 5, 6, 8

[25] Jinshan Pan, Deqing Sun, Hanspeter Pfister, and Ming-Hsuan Yang. Blind image deblurring using dark channel prior. In *CVPR*, 2016. 1, 2, 4, 5, 6

[26] Dongwei Ren, Kai Zhang, Qilong Wang, Qinghua Hu, and Wangmeng Zuo. Neural blind deconvolution using deep priors. In *CVPR*, 2020. 3

[27] William Hadley Richardson. Bayesian-based iterative method of image restoration. *JoSA*, 62(1):55–59, 1972. 3

[28] Jaesung Rim, Haeyun Lee, Jucheol Won, and Sunghyun Cho. Real-world blur dataset for learning and benchmarking deblurring algorithms. In *ECCV*, 2020. 4

[29] Qi Shan, Jiaya Jia, and Aseem Agarwala. High-quality motion deblurring from a single image. *ACM ToG*, 27(3):73, 2008. 1, 2, 6

[30] Yu-Wing Tai, Ping Tan, and Michael S Brown. Richardson-lucy deblurring for scenes under a projective motion path. *IEEE TPAMI*, 33(8):1603–1618, 2010. 3

[31] Xin Tao, Hongyun Gao, Xiaoyong Shen, Jue Wang, and Jiaya Jia. Scale-recurrent network for deep image deblurring. In *CVPR*, 2018. 2, 3, 4, 5, 6

[32] Oliver Whyte, Josef Sivic, and Andrew Zisserman. Deblurring shaken and partially saturated images. *IJCV*, 2014. 1, 2, 3, 7, 8

[33] Li Xu and Jiaya Jia. Two-phase kernel estimation for robust motion deblurring. In *ECCV*, 2010. 6

[34] Li Xu, Shicheng Zheng, and Jiaya Jia. Unnatural l_0 sparse representation for natural image deblurring. In *CVPR*, 2013. 1, 2, 4, 6

[35] Yanyang Yan, Wenqi Ren, Yuanfang Guo, Rui Wang, and Xiaochun Cao. Image deblurring via extreme channels prior. In *CVPR*, 2017. 1, 2

[36] Lu Yuan, Jian Sun, Long Quan, and Heung-Yeung Shum. Progressive inter-scale and intra-scale non-blind image deconvolution. *Acm ToG*, 27(3):1–10, 2008. 3

[37] Hongguang Zhang, Yuchao Dai, Hongdong Li, and Piotr Koniusz. Deep stacked hierarchical multi-patch network for image deblurring. In *CVPR*, 2019. 2, 3

[38] Jiawei Zhang, Jinshan Pan, Jimmy Ren, Yibing Song, Linchao Bao, Rynson WH Lau, and Ming-Hsuan Yang. Dynamic scene deblurring using spatially variant recurrent neural networks. In *CVPR*, 2018. 3